Proteome-scale Isolation and Tagging of P Granules Uncover Unique Solid-like Condensates to Ensure Spermatogenesis

Xuanxuan Guo,[1,2,3] Xuejia Li,[1,2,3] Lin Zeng,[4] Lili Li, [1,2,3] Di Rao,[1,2,3] Long Miao,[5,6,7,8] Shikui Tu,[4*] En-Zhi Shen[1,2,3*]

[1]Key Laboratory of Growth Regulation and Transformation Research of Zhejiang Province, School of Life Sciences, Westlake University, Hangzhou, Zhejiang, China

[2]Westlake Laboratory of Life Sciences and Biomedicine, Hangzhou, Zhejiang, China

[3]Institute of Biology, Westlake Institute for Advanced Study, Hangzhou, Zhejiang, China

[4]Centre for Cognitive Machines and Computational Health (CMaCH), School of Computer Science, Shanghai Jiao Tong University, Shanghai, China.

[5]Key Laboratory of RNA Biology, CAS Center for Excellence in Biomacromolecules, Institute of Biophysics, Chinese Academy of Sciences, Beijing 100101, China.

[6]University of Chinese Academy of Sciences, Beijing 100049, China.

[7]Center for Biological Imaging, Core Facilities for Protein Science, Institute of Biophysics, Chinese Academy of Sciences, Beijing 100101, China.

[8]MOE Key Laboratory of Cell Proliferation and Regulation Biology, College of Life Sciences, Beijing Normal University, Beijing 100875, China.

*Correspondence: tushikui@sjtu.edu.cn(S.-K.T), shenenzhi@westlake.edu.cn (E.-Z.S.)

ABSTRACT

P granules are membrane-less organelles essential for germ cell fate specification, post-transcriptional regulation, and genome stability. However, the molecular organization and developmental plasticity of P granules remain incompletely understood. Here, we isolated P granules from enriched *C. elegans* germ cells and identified 256 associated proteins by mass spectrometry. Using CRISPR/Cas9 together with programmatically generated primer sets, we established a proteome-scale collection of endogenously tagged strains for visualizing P-granule proteins. The corresponding fluorescence imaging data, together with genome-wide primer sets for constructing endogenously tagged *C. elegans* strains, were integrated into an annotated, searchable online database (https://scgerm-atlas.sjtu.edu.cn/website/#/P-granules). Using this resource, we systematically visualized P-granule protein dynamics and mapped their spatiotemporal expression trajectories during gametogenesis. Following the remodeling of perinuclear P granules during spermatogenesis, a distinct set of male-specific germ granules emerged, that likely forms diverse solid-like condensates to meet the multifaceted physiological demands of spermatogenesis. Together, this work uncovers a developmental transition in germ granule composition and highlight their critical role in male fertility and germline integrity, laying the groundwork for future studies on germ granules in development and disease.

KEYWORDS

C. elegans, Germ granules, P granules, Proteomics, Endogenous fluorescent tagging, Spermatogenesis.

INTRODUCTION

Germ granules are membraneless organelles (MLOs) that are uniquely present in germ cells and widely conserved across the animal kingdom[1]. They play essential roles in germ cell fate determination, post-transcriptional regulation, and maintenance of germline homeostasis[2]. Elucidating the protein composition and functions of germ granules is therefore fundamental for understanding how germ cells preserve their identity and functionality, and also offer insights into the molecular basis of infertility and related reproductive disorders. P granules are *C. elegans* specific germ granules composed of proteins and RNAs that form liquid-like condensates. During early embryogenesis, P granules localize to the germline precursor cells Z2 and Z3 through asymmetric cytoplasmic segregation and subsequently attach to the perinuclear region of germ cells, where they are present in all germ cells except mature sperm[3,4]. Functionally, P granules participate in post-transcriptional gene regulation, including mRNA stabilization and translational repression, thereby contributing to germ cell fate determination, gametogenesis, and the maintenance of germline integrity[5-7]. Owing to their well-defined localization patterns, tractable genetics, and evolutionarily conserved core components, *C. elegans* P granules have become an ideal model for dissecting the molecular composition, assembly mechanisms, and biological functions of germ granules.

Since the 1980s, when Susan Strome and Bill Wood first observed germ-cell-specific cytoplasmic granules in *C. elegans* [8], genetic approaches such as chemical mutagenesis and RNAi screening have progressively elucidated the molecular composition and functional framework of P granules[9-12]. In recent years, advances in mass spectrometry-based proteomics and proximity-labeling have greatly accelerated the exploration of P granule composition. For example, Price *et al.* used TurboID combined with RNAi screening to identify EGGD-1 and EGGD-2 as critical for perinuclear anchoring, while Zhao *et al.* further refined the approach to identify[13-15] HERD-1 as a regulator linking condensate assembly to small RNA-mediated transgenerational inheritance. Although these studies have broadened our understanding of the P granule proteome, they still rely primarily on indirect approaches. In contrast, recent advances have enabled the direct biochemical purification of other membraneless organelles, such as cytoplasmic stress granules and P bodies, allowing comprehensive analyses of their composition and function[16,17]. However, the biochemical purification of P granules remains challenging. Therefore, developing a robust purification strategy for P granules to enable systematic molecular characterization has become a pressing goal.

Among the various types of germ granules formed during reproduction, those in female germ cells have been extensively studied across species. These granules can be broadly classified into three categories: embryonic germ granules, which are essential for germ cell specification; oocyte-specific granules, such as

the Balbiani body, which associate with mitochondria and contribute to oocyte polarity; and perinuclear germ granules (also known as the nuage), found in differentiating germ cells and playing a central role in genome surveillance within the germline[18,19]. In contrast, P granules were observed to disassemble and disappear during spermatogenesis, a phenomenon long attributed to the extensive cytoplasmic reduction that occurs during sperm differentiation[7]**.** However, in 2022, Jan Schreier and colleagues identified a distinct type of germ granule, termed the PEI granule, which persists throughout spermatogenesis—including in round spermatids—and is crucial for paternal epigenetic inheritance and genome protection[20]. This discovery broadens our understanding of the diversity and functional specialization of germ granules, underscoring that their remodeling and diversification during spermatogenesis remain important directions for future research.

In this study, we developed a method for efficiently purifying perinuclear P granules from highly enriched germ cells of *C. elegans* at the late L4 stage, a developmental phase encompassing spermatogenesis and related germline differentiation processes, identified a total of 256 germ granule protein components. By engineering a proteome-scale resource of endogenously tagged germ granule protein strains, we established spatiotemporal expression trajectories corresponding to germ cell development. The spatiotemporal expression data for P-granule proteins, along with genome-wide primer sets for the construction of endogenously tagged C. elegans strains, are integrated into a searchable web interface. This platform facilitates the generation of strains and enables in vivo visualization and functional analysis of P-granule proteins of interest. Notably, spatiotemporal profiling revealed dozens of previously uncharacterized germ granule proteins that emerge during spermatogenesis. Biophysical and functional characterization of the granules suggests that these newly identified, distinct male-specific components may cooperate to regulate various aspects of spermatogenesis, thereby collectively safeguarding male fertility. Taken together, our study offers a comprehensive view of germ granule dynamics during gametogenesis and provides a valuable resource for future research on male fertility and germ cell development.

RESULTS

Purified P granule proteome uncovered by Label-free Mass Spectrometry

To identify P granule components, we first established a method for isolating high-purity P granules from enriched *C. elegans* germline cells (Figure S1A). In general, our approach involves two significant steps: germ cell isolation and particle sorting. Piwi-family member PRG-1 is a conserved core component of *C. elegans* P granules[21,22]. To label germ cells and germ granules, we integrated green fluorescent protein (GFP) at the N-terminus of PRG-1 using CRISPR/Cas9 (*gfp::tev::2×flag::prg-1*). After germline establishment, P granules remain perinuclear and are closely associated with the nuclear pore complex. To minimize interference from nuclear membrane components, we used wrmScarlet to label the nuclear membrane protein LMN-1 (*wrmScarlet::lmn-1*). Given the resolution limitations of flow cytometry due to the

small size of germ granules, we introduced SL2 as a linker between GFP and PRG-1, ensuring that GFP expression was PRG-1-dependent in germ cells without GFP localization to germ granules[23,24]. Thue, the experimental strain was *gfp::tev::flag::prg-1; lmn-1::wrmscarlet*, with the *gfp::sl2::flag::prg-1; lmn-1::wrmscarlet* as control (Figure S1B).

P granules are specific to germline cells. To enrich P granules, we first isolated germline cells from synchronized Late L4 stage worms using percoll density gradient centrifugation[25,26]. Confocal imaging revealed a highly enriched population of germline cells, with germ granules clearly visualized. (Figure 1A). After UV crosslinking[27], cells were lysed, and the cytosolic extracts (presorted fraction) were processed by fluorescence-activated cell sorting (FACS). FACS analysis successfully identified wrmScarlet-negative, GFP-positive P granules, maintaining a stable proportion of ~10% (Figure 1B). To verify the purity of the sorted P granules, we first examined the samples using confocal microscopy. The results showed that sorted GFP-positive particles retained their typical size and morphology (Figure 1C). Subsequently, we performed western blot analysis to assess PRG-1 enrichment in different following multiple fractionation steps. After normalizing protein loading based on silver staining, we observed the highest PRG-1 levels in the sorted granules (Figure 1D).

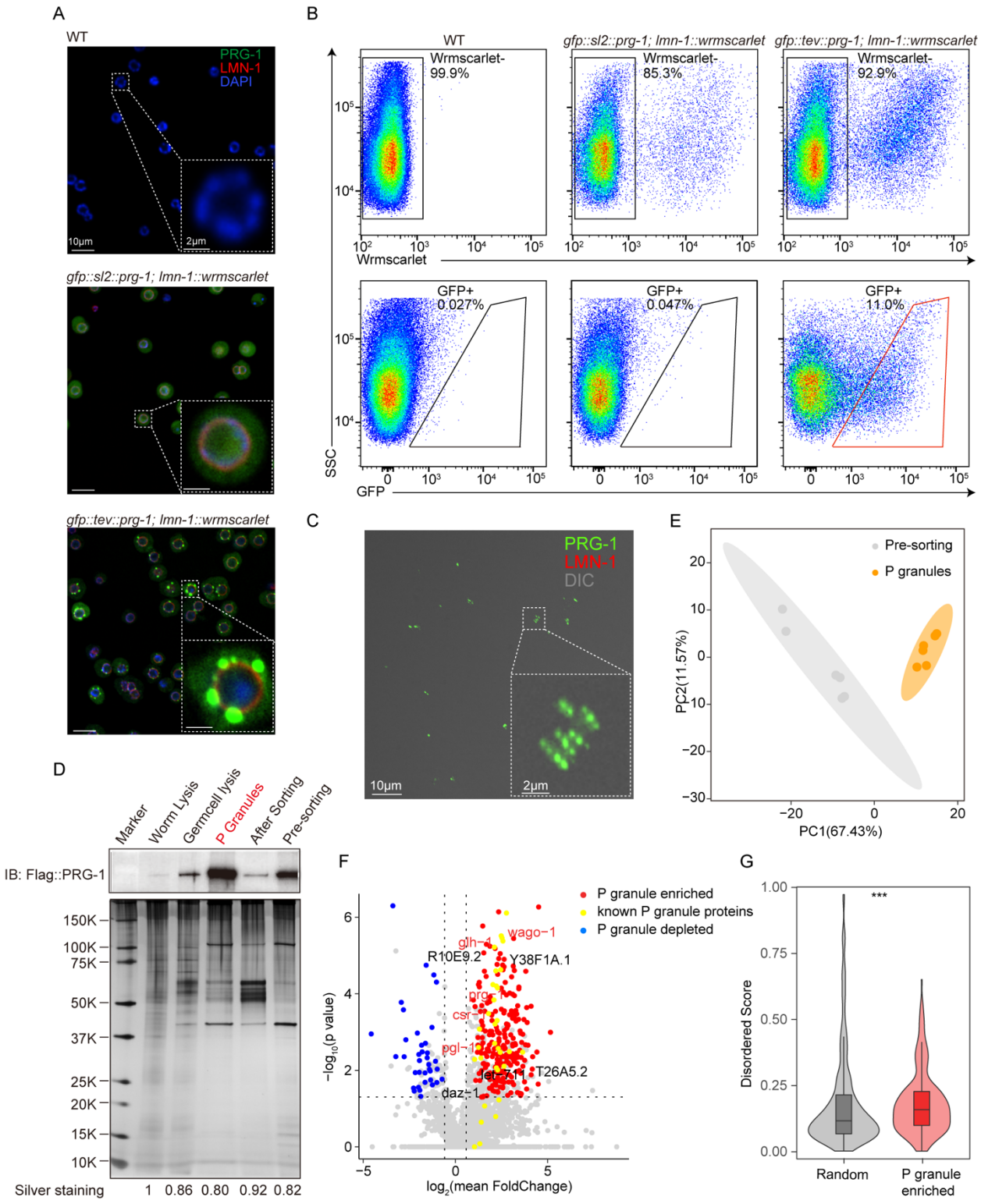

Figure 1: The P granule proteome uncovered by label-free Mass Spectrometry of purified P granule

(A) Representative confocal images of purified germ cells. PRG-1 (green) marks germ granules, LMN-1 (red) labels the nuclear envelope, and DNA is stained blue.

(B) FACS separated particles based on their size and fluorescence. The sorting window of GFP-PRG-1 labeled P granules (right panel) is delineated by the red line. The GFP-SL2-PRG-1 served as a control for non-P granule particles (middle). Wild-type showed only background noise (left).

(C) Representative confocal images of purified P granules.

(D) Western blot verifying the purity of isolated P granule (upper panel). Silver staining shows the protein loading amounts in different samples (lower panel).

(E) Principal component analysis (PCA) of sorted and pre-sorted samples based on six biological replicates.

(F) Volcano plot shows the comparison of protein abundances between sorted and pre-sorted fractions using quantitative values from normalized total spectra of LC-MS/MS. Significantly enriched and depleted proteins (Grey dots) are indicated, as well as known(Yellow dots) and newly validated P granule proteins (Red dots). $p<0.05$; FC>1.5.

(G) Violin plots showing the average intrinsically disordered region (IDR) scores of P granule proteins compared with a random control set predicted by Fldpnn (Wilcoxon-Mann-Whitney test) .***$p<0.001$.

To characterize the protein composition of perinuclear P granules, liquid chromatography-tandem mass spectrometry (LC-MS/MS) was employed[28]. Principal component analysis (PCA) indicated that six biological replicates from the same group clustered together, confirming the reproducibility of the mass spectrometry data (Figure 1E). Subsequently, comparing protein relative abundances between the sorted and pre-sorted fractions, we identified 256 proteins as significantly enriched in P granules (Fisher exact test, $p < 0.05$) (Figure 1F; Table S1). As expected, functional enrichment analysis identified these proteins as being involved in post-transcriptional gene regulation, gametogenesis, and negative regulation of gene expression. Among the 256 proteins, 35 were previously known as P granule components (Table S1), and 159 exhibited evolutionary conservation (Figure S1D). Of particular note, 157 proteins remain totally unannotated. Additionally, predictive analyses indicated a significant enrichment of intrinsically disordered regions (IDRs) in P granule proteins relative to controls (Figure 1G), suggesting a potential role of IDRs in granule assembly and function. Functional enrichment indicated that the 256 identified P-granule proteins participate mainly in post-transcriptional regulation, gametogenesis, and non-membrane-bounded organelle assembly (Figure S1C). The enrichment patterns align well with known germ-granule functions, underscoring the reliability of our proteomic dataset. Taken together, we identified 256 constituent proteins from the isolated P granules.

Visualizing the P granule proteome through engineering of proteome-scale endogenously tagged strains

To gain deeper insights into the distribution of germ granule components identified by mass spectrometry, endogenous fluorescent tagging was applied to the full set of identified germ granule proteins. To construct endogenously fluorescently labeled germ granule protein strains, we utilized CRISPR/Cas9 gene editing methods, employing unc-119 as a selectable marker for integration screening[29,30]. The workflow is depicted

158 in Figure S2E. For co-localization analysis, we chose a key scaffolding protein PGL-1 which is required for
159 P granule assembly as a marker[10] (Figure S2A and S2B). We selected the GGS-GFP-TEV-FLAG-AID multi-
160 functional tag to label the proteins (Figure S2C). Fluorescent protein insertion sites (N- or C-terminus) were
161 selected based on literature or defaulted to the C-terminus when no reference was available. Primers
162 required for plasmid construction in transgenic *C. elegans* were batch-retrieved computationally (Table S2).
163 In total, 137 tagged strains were generated, 95 (75%) of which were detectable by fluorescence imaging.
164 Of these, 87 proteins formed granule-like condensates and co-localized with PGL-1(Figure 2A). For
165 example, Y66D12A.19, a protein stably expressed in germ cells, formed granule-like structures surrounding
166 the nucleus and co-localized with PGL-1 (Figure 2B). So far, we have further confirmed the accuracy of the
167 identified P granule proteins. Therefore, hundreds of new germ granule protein components, along with
168 their expression and localization patterns, are likely to be uncovered.

169 To facilitate access to the original fluorescence images of P granules proteins and retrieval of primer sets
170 for generating user-defined transgenic C. elegans strains, we compiled these data into a searchable online
171 database available at https://scgerm-atlas.sjtu.edu.cn/website/#/primer. The main functions and
172 representative interfaces of the database are shown in Figure S3.

173

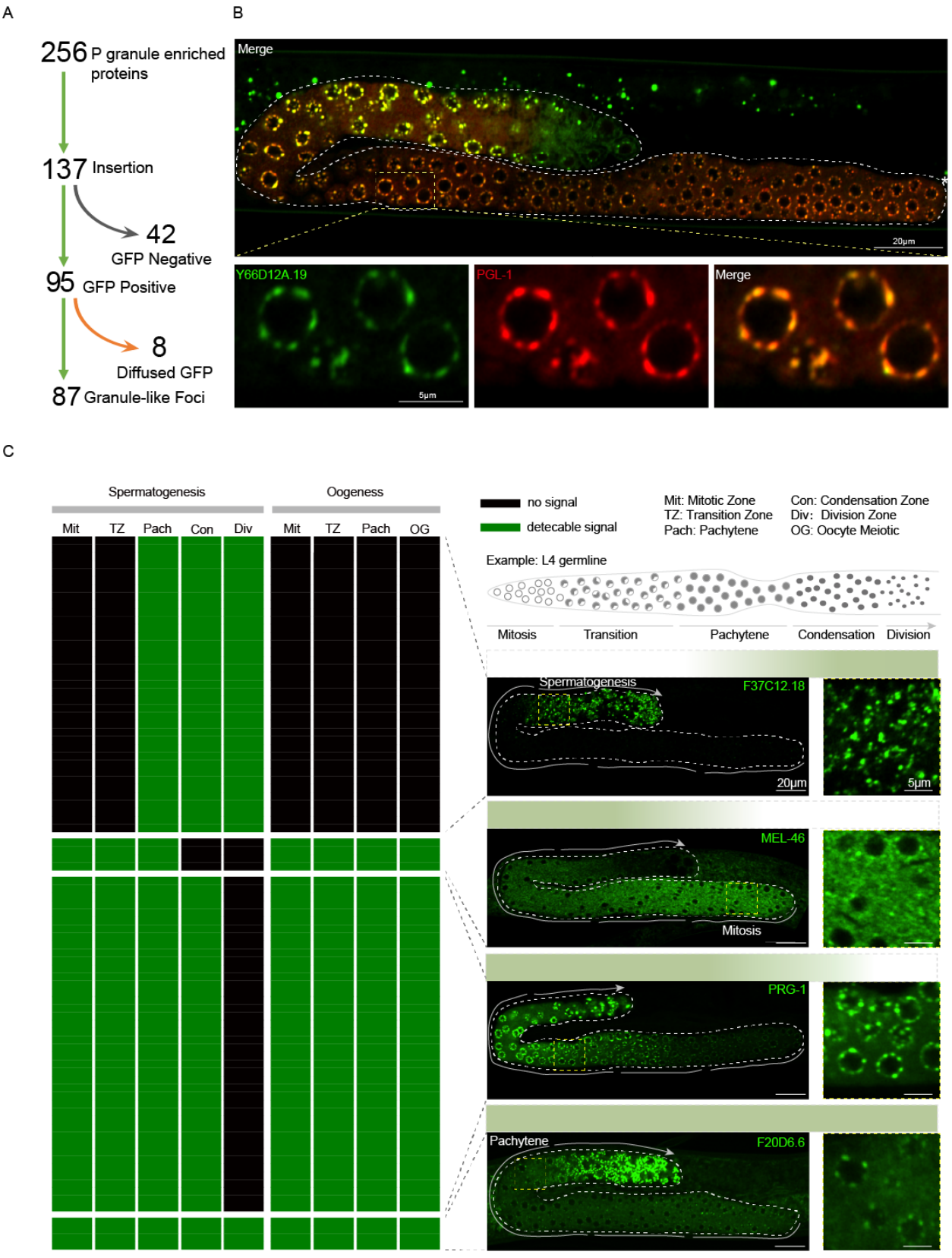

Figure 2: Endogenous fluorescent tagging reveals dynamic expression trajectories of P granule proteins during gametogenesis

(A) Summary of the construction of endogenously fluorescently tagged P granule protein strains.

(B) Representative confocal images of the endogenously labeled P granule component Y66D12A.19 showing its localization to P granules.

(C) Heatmap showing expression trajectories of 87 granule proteins during germ cell development. Black squares indicate no signal, and green squares indicate detectable signal. Representative images and corresponding magnified views are shown on the right.

P granules exhibit developmentally related compositional remodeling during gametogenesis

To gain deeper insights into the compositional changes, granule dynamics, and germ cell development of germ granule components, we systematically analyzed the developmental expression trajectories of P granule proteins identified by mass spectrometry, we used confocal microscopy to analyze the expression pattern of the labeled proteins systematically during gametogenesis. Spanning two developmental processes, images were classified into five stages for spermatogenesis (mitotic, transition zone, pachytene, condensation, and division zones) or four stages for oogenesis (mitotic, transition zone, pachytene, and oogenic stages). The frequency distribution of distinct expression patterns was manually scored to generate specific expression trajectories. Based on these scores, 87 proteins were clustered into four groups. According to the heatmap, P-granule components exhibit distinct spatiotemporal expression dynamics during germ cell development, particularly throughout spermatogenesis (Figure 2C; Table S3). Unlike previous assumptions, we found that spermatogenesis is accompanied by a coordinated compositional transition of germ granules, in which mitotic P-granule proteins are gradually displaced and replaced by sperm-specific factors, reflecting a developmentally regulated remodeling of granule architecture. By the way, those tagged P granule proteins during oogenesis fall into two major groups: participating and non-participating components.

In 2018, Tzur *et al.* generated a spatiotemporal transcriptomic map of *C. elegans* gonads, providing a valuable resource for germline expression analysis[31]. To gain transcriptomic insights into the expression dynamics of germ-granule components during gametogenesis, we analyzed the mRNA expression profiles of 256 identified proteins in both hermaphrodites and males. Hierarchical clustering of germ-granule genes based on their transcriptomic profiles revealed several distinct expression groups across gametogenesis (Figure S2F; Table S4). Two major groups were predominantly expressed during spermatogenesis, comprising largely uncharacterized genes together with those linked to phosphorylation and signal-transduction pathways. Another broad cluster showed sustained expression during oogenesis but was repressed during spermatogenesis, enriched for factors involved in gene silencing, translational regulation, and oocyte development. A smaller set of genes maintained stable expression across both gametogenic programs, functioning mainly in ncRNA-mediated post-transcriptional regulation, whereas a few exhibited

meiotic or embryonic enrichment. Together, these data uncover distinct transcriptional trajectories of germ-granule components, underscoring a coordinated remodeling that accompanies gametogenesis and reflecting their potential functional specialization. Overall, this compositional remodeling in both protein and transcriptional level likely reflects a functional specialization of germ granules to meet the translational and regulatory demands of germ cell differentiation and provides key insights into the roles of individual granule genes.

Male-specific germ granules arise following the transition of perinuclear P granules.

Proteomic and transcriptomic analyses identified dozens of previously uncharacterized germ-granule genes whose expression initiates in perinuclear P granules at the L4 pachytene stage and continues throughout spermatogenesis (Figure S4A and S4B). To test whether sperm-specific germ granules are required for reproduction, we generated CRISPR/Cas9 null alleles for 20 candidates and measured the progeny number. All mutants exhibited reduced fertility, though the extent of reduction varied among strains (Figure 3A). These findings underscore the essential role of germ granule components expressed during spermatogenesis in maintaining the reproductive competence of *C .elegans*. Among the genes analyzed, the knockout of C18E3.1 exhibited the most significant detrimental effect on the reproductive capacity of *C. elegans*.

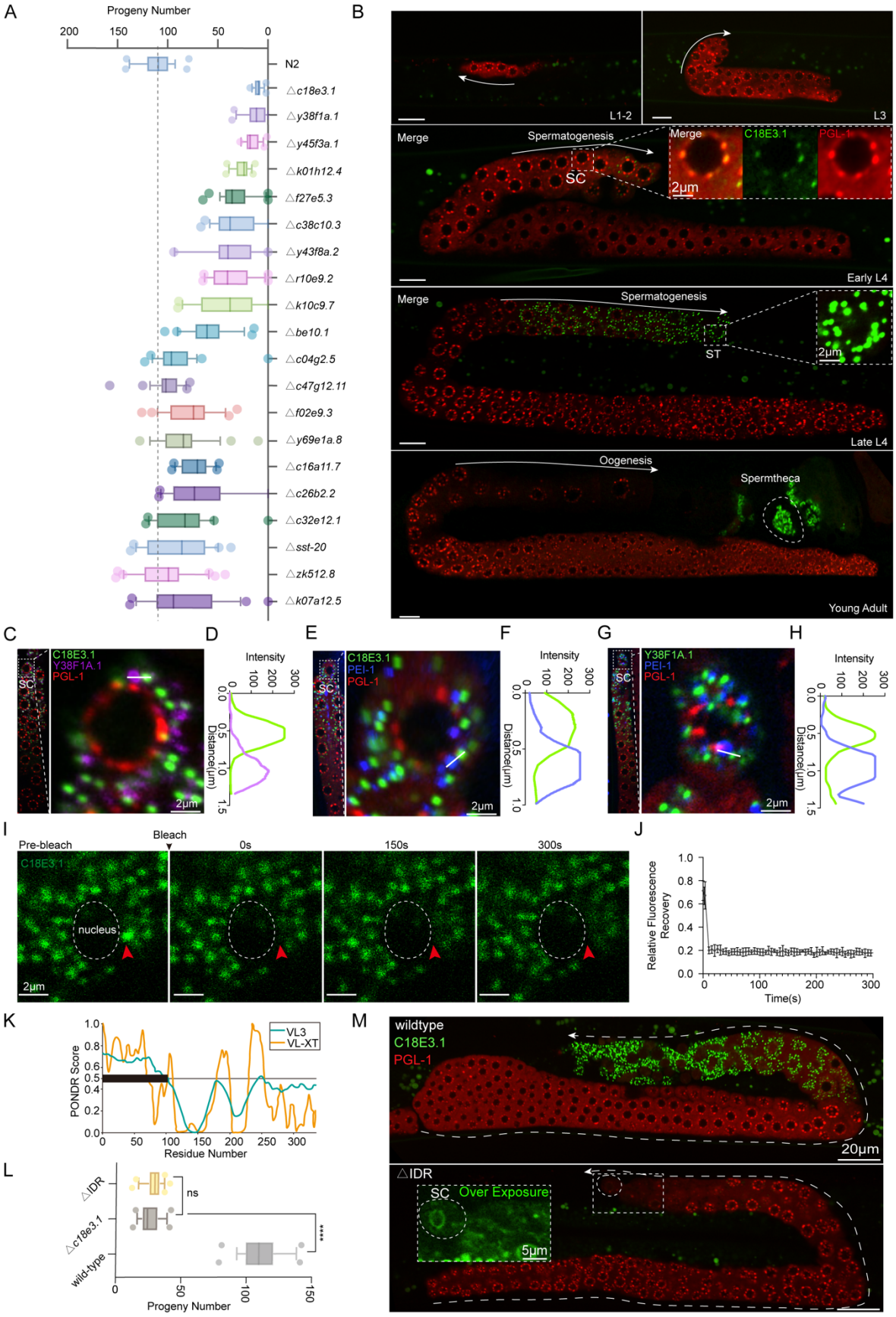

Figure 3. Multiple functional germ granules formed during spermatogenesis.

(A) Progeny numbers of sperm-specific Germ Granule protein-deficient strains compared with wild-type. The dashed line represents the median value of the control group.

(B) Representative confocal images showing the expression pattern of C18E3.1 across development. *pgl::wrmScarlet* serves as P granule marker. Scale bars: 10 μm.

(C-H) Representative confocal images showing the subcellular localization of two sperm-specific germ granule proteins in spermatocytes (SC), *pgl-1::wrmScarlet* serves as P granule marker. The white line indicates the position used for fluorescence intensity profiling. The left panel shows the proximal region of the gonad in early L4 worms, and the right panel shows enlarged view of spermatocyte. (D, F,H) the right panel shows the fluorescence intensity along the white line in (C, E and G). (C, D) C18E3.1 (green) and Y38F1A.1 (purple). (E, F) C18E3.1 (green) and PEI-1 (blue). (G, H) Y38F1A.1 (green) and PEI-1 (blue).

(I) Time-lapse confocal images showing fluorescence recovery of C18E3.1 after photobleaching.

(J) Quantification of FRAP results. Data were obtained from five cells per group and are presented as mean ± SEM (error bars).

(K) C18E3.1 domain composition. Prediction of intrinsically disordered regions was performed using PONDR VSL2 and PONDR VL3 algorithms.

(L) Brood size of wild-type and C18E3.1 variants. ****p<0.0001, two-tailed Student's t-test.

(M) Confocal images of late-L4 stage hermaphrodites expressing indicated proteins. In all images: Green: C18E3.1, Red: PGL-1. Images represent two biologically independent experiments. Scale bars: 20 μm.

To be more specific, we used C18E3.1 as an example to characterize sperm-specific germ granules. As described, C18E3.1 initially co-localizes with PGL-1 during the early stages of expression and forms more condensates gradually in the cytoplasm over time (Figure 3B). A similar localization pattern was observed for the other candidate protein, Y38F1A.1 (Figure S4C). These results suggest that P granules may undergo a developmental transition and remodeling during spermatogenesis. P granules are widely recognized for their liquid-like properties. To further assess the phase separation behavior of C18E3.1 condensates, FRAP assays were performed[32]. The results showed negligible fluorescence recovery within 5 minutes, indicating that C18E3.1 condensates are largely immobile and exhibit a low-dynamic state (Figure 3I and 3J). Intrinsically disordered regions (IDRs) often play a central role in promoting condensate formation[33]. Sequence analysis predicted that the N-terminal region of C18E3.1 constitutes an IDR (Figure S4K). Consistent with this, domain-deletion mutant strains were generated in the *c18e3.1::gfp* background to assess the functional relevance of the IDR in sperm granule assembly (Figure 3L), and loss of the IDR resulted in reproductive defects similar to those observed in the *c18e3.1* knockout. Fluorescence imaging revealed that deletion of the IDR markedly reduced granule formation during spermatogenesis, leading to diffuse cytoplasmic GFP signals (Figure 3M). Consistent with C18E3.1, Y38F1A.1 also contains a predicted

N-terminal IDR, and its deletion impaired the formation of solid-like condensates and caused fertility defects similar to those of the Y38F1A.1 knockout strain (Figure S4D-S4H). Together, these findings demonstrate that the IDR region contributes to the assembly of solid-like sperm specific condensates with limited molecular mobility.

To test whether the identified sperm-specific proteins assemble into the same condensate, we selected another candidates Y38F1A.1 together with C18E3.1 for colocalization analysis (Figure 3D). Colocalization experiments using worms co-expressing C18E3.1::GFP and Y38F1A.1**::**mCardinal revealed that the two proteins were spatially segregated, suggesting that they form distinct condensates. Given that a previous study reported a PEI-1 mediated condensate associated with heredity during spermatogenesis, we next examined whether this structure corresponds to the sperm-specific granules identified here. Colocalization analyses in C18E3.1::GFP; PEI-1::BFP and Y38F1A.1::GFP; PEI-1::BFP worms showed that C18E3.1, Y38F1A.1, and PEI-1 occupy distinct, non-overlapping regions(Figure 3E and 3F)**.** These findings demonstrate that multiple compositionally and spatially distinct germ granules are assembled during spermatogenesis, highlighting their potential functional diversification. Taken together, these results demonstrate that male specific germ granules form along with the compositional remodeling of liquid-like P granules and progress into functional condensates characterized by low molecular dynamics.

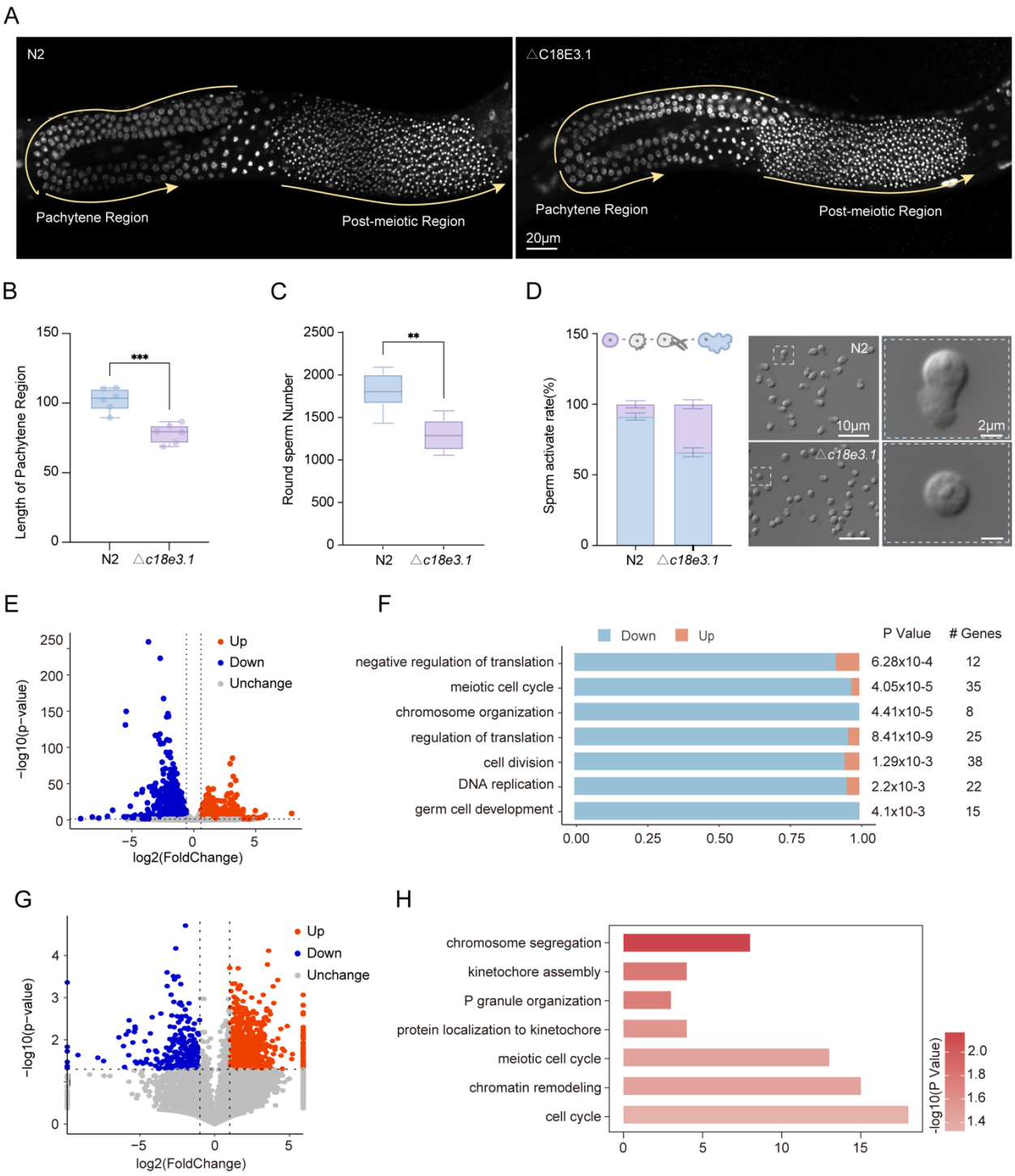

Figure 4. Loss of the sperm-specific germ granule protein C18E3.1 impairs spermatid formation and activation.

(A) Confocal images of gonads from adult male worms (WT and *c18e3.1* mutants).

(B) Quantification of pachytene region length in WT and *c18e3.1* mutants.

(C) Quantification of round spermatid numbers in WT and *c18e3.1* mutants.

(D) In vitro sperm activation assay in WT and *c18e3.1* mutants. Activated sperm are shown in blue.

(E) Volcano plot of the significantly dysregulated genes detected by mRNA-seq. |log2 fold-change>1.25, FDR<0.05).

(F) Gene Ontology (GO) enrichment analysis of dysregulated genes shown in (E) (FDR<0.05).

(G) Volcano plot of the significantly dysregulated genes detected by Ribo-seq. (log2 fold-change>1.25, FDR<0.05)

(H) Gene Ontology (GO) enrichment analysis of upregulated genes shown in (G) (FDR<0.05).

Male-specific germ granules modulate spermatogenesis

Given their specific expression pattern, sperm-specific germ granules were hypothesized to contribute to spermatogenesis. To define the role of C18E3.1 during spermatogenesis, we analyzed sperm development in *c18e3.1* knockout males. Males were generated by heat shock for subsequent analysis. DAPI staining revealed that the gonad arms, particularly the pachytene region, were markedly shortened in *c18e3.1* mutants compared with wild type (Figure 4A and 4B). Quantification of sperm production showed a marked reduction in round spermatids (Figure 4C), and in vitro activation assays demonstrated a significant decrease in sperm activation rate relative to wild type (Figure 4D). These findings demonstrate that sperm-specific germ granules coordinate spermatid differentiation and activation, which are essential for male fertility in *C. elegans*. To elucidate the molecular basis of sperm maturation defects observed in *c18e3.1* knockout strains, we performed transcriptomic analysis (Table S5). This analysis revealed widespread gene expression alterations, with more than a thousand genes differentially expressed. GO enrichment analysis indicated that downregulated genes were predominantly involved in negative regulation of translation and meiotic progression (Figure 4E and 4F). This suggests that the loss of *c18e3.1* may impair translational homeostasis, potentially leading to aberrant activation of protein synthesis during spermatogenesis. To evaluate this hypothesis, ribosome profiling was performed to assess translational activity in adult males of the *c18e3.1* knockout strain. The results revealed that, compared to wild-type, over 900 genes exhibited increased translational activity, whereas about 200 showed reduced translation in the knockout samples (Figure 4G; Table S6). Functional enrichment analysis indicated that the upregulated genes largely corresponded to changes observed at the mRNA level (Figure 4H). Therefore, these findings suggest that the sperm-specific germ granule protein C18E3.1 may influence translational regulation and thereby affect the meiotic process during spermatogenesis.

Additionally, we analyzed two other candidate genes that significantly affected reproductive capacity and found that both exhibited similar phenotypic consequences on spermatogenesis. In *y38f1a.1* and *c38c10.3 null allele* worms, spermatid numbers were reduced and sperm activation ability was markedly impaired (Figure S5A and S5B, S5D and S5E). Despite these comparable phenotypes, transcriptomic profiling revealed distinct molecular responses. In *y38f1a.1 knockout group*, downregulated genes were

317 predominantly enriched for nuclear events associated with meiotic division (Figure S5C), whereas in
318 *c38c10.3 mutants* the affected genes were mainly associated with phosphorylation regulation during
319 spermatogenesis (Figure S5F; Table S8). These findings suggest that although both granule components
320 are essential for sperm maturation and activation, they operate through distinct regulatory pathways to fine-
321 tune spermatogenic processes. Collectively, our findings reveal that sperm-specific germ granules share
322 overlapping roles in promoting sperm formation and activation but act through distinct molecular pathways.
323 This functional diversity suggests that different condensates contribute to fine-tune specific aspects of
324 spermatogenesis within the confined cytoplasmic environment of spermatocytes.

325

326 **DISCUSSION**

327 In this study, we established an efficient approach for isolating perinuclear P granules from enriched *C.*
328 *elegans* germ cells, enabling systematic proteomic characterization of their composition and dynamics. This
329 methodological advance provides a valuable platform for dissecting the molecular architecture, assembly
330 principles, and developmental remodeling of germline condensates. Beyond P granules, our strategy offers
331 a broadly applicable framework for the biochemical purification and proteomic analysis of other classes of
332 membraneless organelles. Together with increasing proteomic data on stress granules and P-bodies, the
333 present work expands the repertoire of phase-separated organelles that can be analyzed at the systems
334 level, offering new opportunities to elucidate shared molecular principles governing condensate formation
335 and function[34].

336 Understanding the in vivo dynamics of membraneless organelles during development remains a central
337 challenge in cell biology. *C. elegans* provides a uniquely powerful system to address this question, as its
338 germ granules are optically accessible throughout development and amenable to endogenous fluorescent
339 tagging. Based on our proteomic map, we generated 137 endogenously tagged strains covering a broad
340 range of germ granule components, which allowed us to visualize their spatiotemporal expression patterns
341 in living animals. These strains serve as a comprehensive resource for studying granule dynamics in germ
342 cell differentiation and for uncovering how protein composition correlates with developmental stage and cell
343 fate.

344 Our results reveal pronounced developmental plasticity of germ granule composition. Systematic profiling
345 across germline stages showed that the identities and abundances of granule-associated proteins change
346 dynamically, and that male and female gametogenesis display strikingly divergent expression trajectories.
347 This compositional remodeling likely reflects a functional reprogramming of germ granules from maintaining
348 germline identity to supporting gamete-specific differentiation[35,36]. The temporal correlation between stage-
349 specific expression and cell fate transition underscores the idea that condensate composition itself can act
350 as a readout—or possibly a driver—of developmental state. These findings highlight the complexity and
351 adaptability of the germ granule network as a regulatory platform for germ cell maturation.

While most previous studies of germ granules have focused on embryogenesis or oogenesis, our work identifies and characterizes a previously underexplored class of sperm-specific germ granules. These structures arise as canonical perinuclear P granules progressively disassemble during meiosis, accompanied by the sequential emergence of new condensates composed of sperm-specific proteins. In the early L4 germline, when spermatocytes first enter the pachytene stage, we observed partial spatial overlap between P granule components and the newly appearing sperm-specific markers, consistent with a transitional remodeling process. This stage coincides with the reported decline and eventual disappearance of canonical P granule components such as PGL-1 and GLH-1. Together, these observations suggest a developmentally ordered handover in which the disassembly of P granules is coupled to the assembly of sperm-specific condensates, representing a reorganization of the germline condensate system in response to meiotic and transcriptional reprogramming.

Colocalization analyses further demonstrated that distinct sperm granule components, such as C18E3.1 and Y38F1A.1, occupy non-overlapping regions, implying the existence of multiple, compositionally independent condensates during spermatogenesis. This spatial segregation contrasts with the close physical coupling among P granules, Z granules, and Mutator foci observed in earlier germline stages[37], suggesting that the germline condensate network becomes more diversified and compartmentalized in male gametes. Functional assays revealed that several of these sperm-specific granule proteins influence fertility to varying degrees, with C18E3.1 showing a particularly strong effect on sperm formation and activation. These findings point to functional specialization among different classes of sperm granules and raise the possibility that they coordinate distinct aspects of sperm maturation and competence.

From a biophysical perspective, germ granules exhibit a continuum of phase states ranging from liquid-like to solid-like, depending on developmental context and physiological conditions. These phase transitions are tightly coupled to cellular fate dynamics, reflecting the distinct physiological demands of different developmental stages. Early embryonic P granules display rapid molecular exchange characteristic of dynamic liquid droplets, enabling them to respond swiftly to fate changes. In contrast, condensates in mature germ cells—such as the Balbiani body or nuage in oocytes are more gel-like or even amyloid-like, reflecting functional requirements for long-term RNA storage and translational repression. In our study, the sperm-specific granule protein C18E3.1 forms condensates through its N-terminal intrinsically disordered region (IDR) and exhibits negligible fluorescence recovery in FRAP assays, indicating a solid-like state. Such low dynamics may help maintain the spatial confinement of regulatory factors, stabilize stored RNAs or proteins, and protect critical developmental information in transcriptionally quiescent sperm. We propose that the formation of these solid-like granules represents an adaptation for maintaining sperm potential and epigenetic integrity during prolonged storage.

In summary, our work provides a comprehensive molecular and developmental framework for understanding dynamic behavior of germ granules during gametogenesis in *C. elegans*. By integrating biochemical purification, proteomic profiling, and live imaging, we uncover a stepwise transition in which

388 canonical P granule components are orderly dismantled during meiosis and replaced by sperm-specific
389 condensates with distinct molecular compositions and biophysical properties. This remodeling exemplifies
390 how phase-separated organelles can be dynamically repurposed to meet the developmental and
391 physiological needs of differentiating gametes. Future studies combining high-resolution imaging, RNA
392 profiling, and perturbation genetics will be essential to elucidate the molecular triggers and regulatory logic
393 that govern this condensate transition and its roles in sperm differentiation and fertility.

394

STAR★METHODS

METHOD DETAILS

Strains and Maintenance

All of the *C. elegans* strains were maintained at 20°C on nematode growth medium (NGM) plates and seeded with Escherichia coli OP50, as described previously [38]. Null alleles were generated using CRISPR/Cas9 RNP methods previously described [39], by co-injection of Cas-9 RNPs, donors (oligos and melted PCR products) and rol-6 marker. Endogenously fluorescent-tagged strains were generated using a plasmid-based CRISPR/Cas9 system with *unc-119(ed4)* as a selection marker[29,30].

Fertility of *C. elegans*

Synchronized populations were bleached and plated on NGM plates with OP50 at 25°C. Brood size was determined by counting the number of F_1 larvae produced by individual hermaphrodites. At least 15 animals were analyzed per strain.

Microscopic imaging of P granule components

Images of GFP-tagged P granule components were acquired using an Andor Dragonfly confocal microscope. Live animals were immobilized on glass slides (Thermo) with 1 mM levamisole. Images were further processed and cropped by Imaris programs.

P Granule Purification

Synchronized late L4-stage worms were grown on OP50-seeded NGM plates at 20 °C for 50 h. The collected populations were washed three times with M9 buffer, followed by two washes with sterile ddH_2O. For cuticle permeabilization, worm pellets were treated with three volumes of SDS–DTT solution (20 mM HEPES, 0.25% SDS, 200 mM DTT, 3% sucrose, pH 8.0) for 4–5 min, followed by five washes with egg buffer (118 mM NaCl, 48 mM KCl, 2 mM $CaCl_2$, 2 mM $MgCl_2$, 25 mM HEPES, pH 7.3). The worms were then digested with two volumes of pronase E (15 mg/mL in egg buffer) for 25 min with gentle shaking. The digestion was stopped by adding egg buffer containing 10% FBS, and the cells were washed three times. Germ cells were purified by Percoll density-gradient centrifugation using 90%, 70%, and 50% layers prepared in egg buffer. After centrifugation at 800 × g for 20 min, cells collected from the 90–70% interface were recovered as purified germ cells for downstream applications.

Cell pellets were frozen and stored at −80 °C. Unless otherwise stated, all subsequent procedures were carried out at 4 °C or on ice. Pellets were resuspended in lysis buffer (50 mM Tris-HCl, pH 7.4, 1 mM EDTA, 150 mM NaCl, 0.2% Triton X-100) supplemented with 65 U/mL RNaseOUT ribonuclease inhibitor (Promega) and an EDTA-free protease inhibitor cocktail (Roche Diagnostics). To enhance lysis efficiency, the suspension was disrupted on an Eppendorf benchtop shaker at 1,500 rpm for 20 min. The lysate was centrifuged at 200 × g for 5 min to remove nuclei. To eliminate residual DNA, the supernatant was supplemented with 10 mM $MgSO_4$ and 1 mM $CaCl_2$ and treated with 4 U/mL RQ1 DNase (Promega) for 30

min at room temperature. The resulting supernatant was centrifuged again at 10,000 × g for 7 min, and the pellet was resuspended in 40 µL lysis buffer containing 80 U RNaseOUT. This organelle-enriched 10,000 × g fraction was referred to as the pre-sorted fraction**.** P granules were subsequently isolated from this fraction by fluorescence-activated particle sorting using a Cytoflex SRT cell sorter (Beckman). Particles were detected based on forward-scattered light (FSC) and GFP fluorescence, using a 488 nm excitation laser (526/52 nm band-pass filter) and a 561 nm excitation laser (561/19 nm band-pass filter).

Western Blot

Samples were homogenized in SDS lysis buffer at 95°C for 10 minutes. Lysates were centrifuged at 12000rpm for 10 minutes to obtain protein supernatant. Proteins (100 µg) were resolved by SDS-PAGE and transferred to PVDF membranes (BioRad). Mouse anti-Flag antibody (Sigma, 1:5000) and HRP goat anti-mouse igG(Immunology, AE012,1:10000) were used for probing the blots.

Proteomics

After matching concentrations of the P granule sorted and pre-sorted fractions, samples were processed for liquid chromatography–tandem mass spectrometry (LC-MS/MS) in the Proteomics and Metabolomics platform of Westlake University. Peptides were analyzed on a Thermo Vanquish Neo nano-HPLC system coupled to a Thermo Exploris 480 mass spectrometer equipped with a FAIMS Pro interface. Peptide separation was achieved on a C18 analytical column using a 60-min gradient at a flow rate of 0.3 µL/min. The mass spectrometer was operated in data-dependent acquisition mode using Xcalibur 4.1 software, with FAIMS compensation voltages of −45 V and −65 V applied as two independent acquisition events. MS data were processed with Thermo Xcalibur Qual Browser and Proteome Discoverer software against the *C. elegans* UniProt proteome database. Database searches were performed using Sequest with a 10 ppm precursor tolerance and a 0.02 Da fragment tolerance. Peptide identifications were filtered to achieve a 1% false discovery rate (FDR).

mRNA Library Preparation and data analysis

To construct mRNA library, the total RNA of Synchronized worms at L4 stage was extracted by TRIzol regent and followed by ethanol precipitation. Ribosomal RNAs were removed from 1 µg total RNA by using Ribo-off rRNA Depletion Kit (Vazyma, N406). Then, libraries were prepared using VAHTS Universal V8 RNA-seq Library Prep Kit for Illumina (Vazyma, N605), the first-strand cDNA was ligated to 5′ and 3′ adapters of VAHTS Small RNA Library Prep Kit for Illumina (Vazyma, NR801). Finally, the libraries were amplified with a barcoded PCR primer for 14 cycles. Sequencing was performed on an Illumina HiSeq 2000. RNA-seq reads were trimmed with Cutadapt and aligned to the C. elegans genome (WS282) using STAR. Read counts were obtained with featureCounts and normalized in DESeq2 for differential expression analysis. Significance was determined using an adjusted p value < 0.05.

Ribo-seq and data analysis

Ribosome profiling was performed as described [40]. Dissected gonads from synchronized late-L4 C. elegans were collected in ice-cold lysis buffer (20 mM Tris-HCl pH 7.4, 150 mM NaCl, 5 mM $MgCl_2$, 1% Triton X-100, 100 µg/mL cycloheximide, 1 mM DTT, RNase inhibitor). Samples were homogenized using a FastPrep homogenizer at 6.5 m/s for 20 s, and lysates were clarified by centrifugation (20,000×g, 10 min, 4 °C). Supernatants were digested with RNase I, and reactions were stopped with excess RNase inhibitor. Monosomes were isolated by centrifugation through a 1 M sucrose cushion (260,000×g, 3 h, 4 °C; SW55Ti rotor). RNA was extracted from the pellet using TRIzol LS, and 26–34 nt ribosome-protected fragments were purified by 12.5% denaturing PAGE for library construction. Libraries exhibiting CDS enrichment and clear 3-nt periodicity were used for analysis. Adapter sequences and low-quality bases were trimmed with cutadapt, and reads mapping to rRNA were removed using STAR. The remaining reads were aligned to the C. elegans ce11 genome with STAR, and uniquely mapped reads were quantified with featureCounts (Rsubread). Differential expression and translational efficiency analyses were performed using DESeq2 and Xtail, with significance defined as FDR ≤ 0.05. P-site periodicity and read length distributions were evaluated with riboWaltz, and noncanonical ORFs were identified using ORFik based on triplet periodicity evidence.

Statistical analysis

Statistical analysis was performed using GraphPad Prism. Sample sizes and statistical parameters are reported in the main text, figures, and figure legends. Statistical significance was assessed using Student's paired and unpaired t-tests for parametric data, or Wilcoxon rank-sum tests for non-parametric data; p-values ≤ 0.05 were considered statistically significant.

ACKNOWLEDGMENTS

We would like to thank Wei Zou laboratory for their assistance in the construction of the endogenous fluorescently tagged strain of the P granule protein. We thank Dr. Peiguo Yang for insightful suggestions. We thank the Proteomics & Metabolomics Core Facility and the Flow Cytometry Core Facility of Westlake university for technical support. We are grateful to the Beckman Coulter engineering team in Hangzhou for instrument maintenance and assistance. This work was supported by the Zhejiang Provincial Foundation of China (2021R01013), Westlake Education Foundation (041010140118) and National Natural Science Foundation of China (NSFC32070628) to E.-Z.S.

AUTHOR CONTRIBUTIONS

E.-Z.S. conceptualized the study. X.-X.G., X.-J.-L., D.R. and L.-L.L performed the investigation. L.Z developed the online database. L.-L.L. assisted in data analysis. X.-X.G. wrote the original draft. Numerous bacteria and *Caenorhabditis elegans* strains were established by X.-J.-L., L.M provided guidance on experimental design. S.-K.T. provided lots of guidance on bioinformatics. E.-Z.S. reviewed and edited the manuscript.

DECLARATION OF INTERESTS

The authors declare no competing interests.

REFERENCES

1. Eddy, E.M. (1975). Germ plasm and the differentiation of the germ cell line. Int Rev Cytol *43*, 229-280. 10.1016/s0074-7696(08)60070-4.
2. Seydoux, G. (2018). The P Granules of C. elegans: A Genetic Model for the Study of RNA-Protein Condensates. J Mol Biol *430*, 4702-4710. 10.1016/j.jmb.2018.08.007.
3. Hird, S.N., Paulsen, J.E., and Strome, S. (1996). Segregation of germ granules in living Caenorhabditis elegans embryos: cell-type-specific mechanisms for cytoplasmic localisation. Development *122*, 1303-1312. 10.1242/dev.122.4.1303.
4. Updike, D.L., Hachey, S.J., Kreher, J., and Strome, S. (2011). P granules extend the nuclear pore complex environment in the C. elegans germ line. J Cell Biol *192*, 939-948. 10.1083/jcb.201010104.
5. Ouyang, J.P.T., Folkmann, A., Bernard, L., Lee, C.Y., Seroussi, U., Charlesworth, A.G., Claycomb, J.M., and Seydoux, G. (2019). P Granules Protect RNA Interference Genes from Silencing by piRNAs. Dev Cell *50*, 716-728 e716. 10.1016/j.devcel.2019.07.026.
6. Phillips, C.M., and Updike, D.L. (2022). Germ granules and gene regulation in the Caenorhabditis elegans germline. Genetics *220*. 10.1093/genetics/iyab195.
7. Updike, D., and Strome, S. (2010). P granule assembly and function in Caenorhabditis elegans germ cells. J Androl *31*, 53-60. 10.2164/jandrol.109.008292.
8. Strome, S., and Wood, W.B. (1982). Immunofluorescence visualization of germ-line-specific cytoplasmic granules in embryos, larvae, and adults of Caenorhabditis elegans. Proc Natl Acad Sci U S A *79*, 1558-1562. 10.1073/pnas.79.5.1558.
9. Gruidl, M.E., Smith, P.A., Kuznicki, K.A., McCrone, J.S., Kirchner, J., Roussell, D.L., Strome, S., and Bennett, K.L. (1996). Multiple potential germ-line helicases are components of the germ-line-specific P granules of Caenorhabditis elegans. Proc Natl Acad Sci U S A *93*, 13837-13842. 10.1073/pnas.93.24.13837.
10. Kawasaki, I., Shim, Y.H., Kirchner, J., Kaminker, J., Wood, W.B., and Strome, S. (1998). PGL-1, a predicted RNA-binding component of germ granules, is essential for fertility in C. elegans. Cell *94*, 635-645. 10.1016/s0092-8674(00)81605-0.
11. Spike, C.A., Bader, J., Reinke, V., and Strome, S. (2008). DEPS-1 promotes P-granule assembly and RNA interference in C. elegans germ cells. Development *135*, 983-993. 10.1242/dev.015552.
12. Chen, J.X., Cipriani, P.G., Mecenas, D., Polanowska, J., Piano, F., Gunsalus, K.C., and Selbach, M. (2016). In Vivo Interaction Proteomics in Caenorhabditis elegans Embryos Provides New Insights into P Granule Dynamics. Mol Cell Proteomics *15*, 1642-1657. 10.1074/mcp.M115.053975.

13. Branon, T.C., Bosch, J.A., Sanchez, A.D., Udeshi, N.D., Svinkina, T., Carr, S.A., Feldman, J.L., Perrimon, N., and Ting, A.Y. (2018). Efficient proximity labeling in living cells and organisms with TurboID. Nat Biotechnol *36*, 880-887. 10.1038/nbt.4201.

14. Price, I.F., Hertz, H.L., Pastore, B., Wagner, J., and Tang, W. (2021). Proximity labeling identifies LOTUS domain proteins that promote the formation of perinuclear germ granules in C. elegans. Elife *10*. 10.7554/eLife.72276.

15. Zhao, C., Cai, S., Shi, R., Li, X., Deng, B., Li, R., Yang, S., Huang, J., Liang, Y., Lu, P., et al. (2024). HERD-1 mediates multiphase condensate immiscibility to regulate small RNA-driven transgenerational epigenetic inheritance. Nat Cell Biol *26*, 1958-1970. 10.1038/s41556-024-01514-8.

16. Hubstenberger, A., Courel, M., Benard, M., Souquere, S., Ernoult-Lange, M., Chouaib, R., Yi, Z., Morlot, J.B., Munier, A., Fradet, M., et al. (2017). P-Body Purification Reveals the Condensation of Repressed mRNA Regulons. Mol Cell *68*, 144-157 e145. 10.1016/j.molcel.2017.09.003.

17. Wheeler, J.R., Jain, S., Khong, A., and Parker, R. (2017). Isolation of yeast and mammalian stress granule cores. Methods *126*, 12-17. 10.1016/j.ymeth.2017.04.020.

18. Pepling, M.E., Wilhelm, J.E., O'Hara, A.L., Gephardt, G.W., and Spradling, A.C. (2007). Mouse oocytes within germ cell cysts and primordial follicles contain a Balbiani body. Proc Natl Acad Sci U S A *104*, 187-192. 10.1073/pnas.0609923104.

19. Cox, R.T., and Spradling, A.C. (2003). A Balbiani body and the fusome mediate mitochondrial inheritance during Drosophila oogenesis. Development *130*, 1579-1590. 10.1242/dev.00365.

20. Schreier, J., Dietz, S., Boermel, M., Oorschot, V., Seistrup, A.S., de Jesus Domingues, A.M., Bronkhorst, A.W., Nguyen, D.A.H., Phillis, S., Gleason, E.J., et al. (2022). Membrane-associated cytoplasmic granules carrying the Argonaute protein WAGO-3 enable paternal epigenetic inheritance in Caenorhabditis elegans. Nat Cell Biol *24*, 217-229. 10.1038/s41556-021-00827-2.

21. Batista, P.J., Ruby, J.G., Claycomb, J.M., Chiang, R., Fahlgren, N., Kasschau, K.D., Chaves, D.A., Gu, W., Vasale, J.J., Duan, S., et al. (2008). PRG-1 and 21U-RNAs interact to form the piRNA complex required for fertility in C. elegans. Mol Cell *31*, 67-78. 10.1016/j.molcel.2008.06.002.

22. Gu, W., Shirayama, M., Conte, D., Jr., Vasale, J., Batista, P.J., Claycomb, J.M., Moresco, J.J., Youngman, E.M., Keys, J., Stoltz, M.J., et al. (2009). Distinct argonaute-mediated 22G-RNA pathways direct genome surveillance in the C. elegans germline. Mol Cell *36*, 231-244. 10.1016/j.molcel.2009.09.020.

23. Spieth, J., Brooke, G., Kuersten, S., Lea, K., and Blumenthal, T. (1993). Operons in C. elegans: polycistronic mRNA precursors are processed by trans-splicing of SL2 to downstream coding regions. Cell *73*, 521-532. 10.1016/0092-8674(93)90139-h.

24. Evans, D., Zorio, D., MacMorris, M., Winter, C.E., Lea, K., and Blumenthal, T. (1997). Operons and SL2 trans-splicing exist in nematodes outside the genus Caenorhabditis. Proc Natl Acad Sci U S A *94*, 9751-9756. 10.1073/pnas.94.18.9751.

25. Kuhn, S.Z.a.J.R. (2013). Cell isolation and culture. In wormbook, O. Hobert, ed. doi/10.1895/wormbook.1.157.1, http://www.wormbook.org.

26. Hamburger, A.W., Dunn, F.E., and White, C.P. (1985). Percoll density gradient separation of cells from human malignant effusions. Br J Cancer *51*, 253-258. 10.1038/bjc.1985.36.

27. Chodosh, L.A. (2001). UV crosslinking of proteins to nucleic acids. Curr Protoc Mol Biol *Chapter 12*, Unit 12 15. 10.1002/0471142727.mb1205s36.

28. Aebersold, R., and Mann, M. (2003). Mass spectrometry-based proteomics. Nature *422*, 198-207. 10.1038/nature01511.

29. Maduro, M.F. (2015). 20 Years of unc-119 as a transgene marker. Worm *4*, e1046031. 10.1080/21624054.2015.1046031.

30. Kim, H.M., and Colaiacovo, M.P. (2019). CRISPR-Cas9-Guided Genome Engineering in Caenorhabditis elegans. Curr Protoc Mol Biol *129*, e106. 10.1002/cpmb.106.

31. Tzur, Y.B., Winter, E., Gao, J., Hashimshony, T., Yanai, I., and Colaiacovo, M.P. (2018). Spatiotemporal Gene Expression Analysis of the Caenorhabditis elegans Germline Uncovers a Syncytial Expression Switch. Genetics *210*, 587-605. 10.1534/genetics.118.301315.

32. Alberti, S., Gladfelter, A., and Mittag, T. (2019). Considerations and Challenges in Studying Liquid-Liquid Phase Separation and Biomolecular Condensates. Cell *176*, 419-434. 10.1016/j.cell.2018.12.035.

33. Martin, E.W., and Holehouse, A.S. (2020). Intrinsically disordered protein regions and phase separation: sequence determinants of assembly or lack thereof. Emerg Top Life Sci *4*, 307-329. 10.1042/ETLS20190164.

34. Youn, J.Y., Dyakov, B.J.A., Zhang, J., Knight, J.D.R., Vernon, R.M., Forman-Kay, J.D., and Gingras, A.C. (2019). Properties of Stress Granule and P-Body Proteomes. Mol Cell *76*, 286-294. 10.1016/j.molcel.2019.09.014.

35. Seydoux, G., and Braun, R.E. (2006). Pathway to totipotency: lessons from germ cells. Cell *127*, 891-904. 10.1016/j.cell.2006.11.016.

598 36. Pamula, M.C., and Lehmann, R. (2024). How germ granules promote germ cell fate. Nat Rev Genet
599 *25*, 803-821. 10.1038/s41576-024-00744-8.
600 37. Wan, G., Fields, B.D., Spracklin, G., Shukla, A., Phillips, C.M., and Kennedy, S. (2018).
601 Spatiotemporal regulation of liquid-like condensates in epigenetic inheritance. Nature *557*, 679-
602 683. 10.1038/s41586-018-0132-0.
603 38. Brenner, S. (1974). The genetics of Caenorhabditis elegans. Genetics *77*, 71-94.
604 10.1093/genetics/77.1.71.
605 39. Dokshin, G.A., Ghanta, K.S., Piscopo, K.M., and Mello, C.C. (2018). Robust Genome Editing with
606 Short Single-Stranded and Long, Partially Single-Stranded DNA Donors in Caenorhabditis elegans.
607 Genetics *210*, 781-787. 10.1534/genetics.118.301532.
608 40. Singh, M., Cornes, E., Li, B., Quarato, P., Bourdon, L., Dingli, F., Loew, D., Proccacia, S., and Cecere,
609 G. (2021). Translation and codon usage regulate Argonaute slicer activity to trigger small RNA
610 biogenesis. Nat Commun *12*, 3492. 10.1038/s41467-021-23615-w.

611

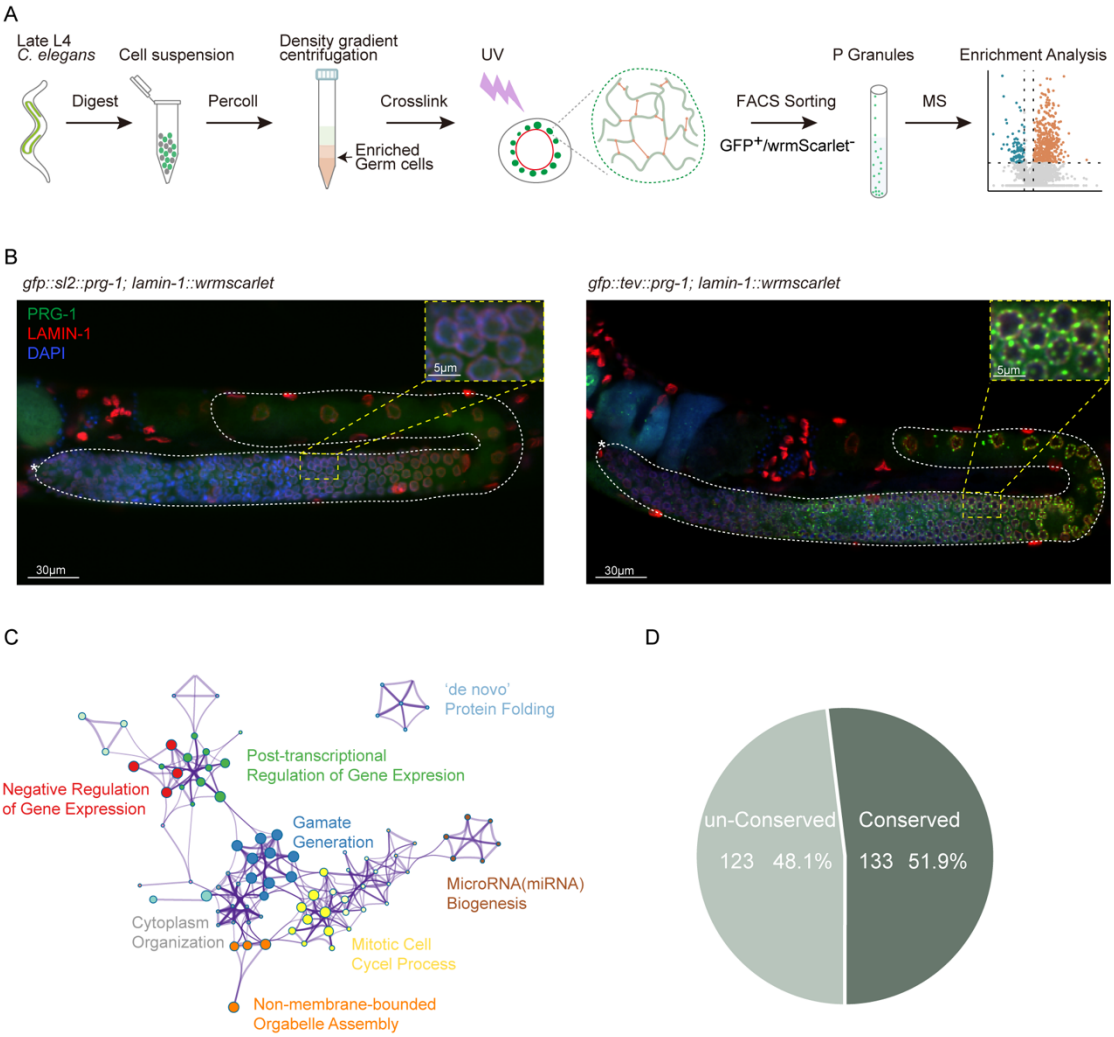

Supplementary Figure 1: Strategy for P granule purification

(A) Workflow for P granule purification.

(B) Representative images of strains for P granule isolation. Left: *gfp::sl2::flag::prg-1;lmn-1::wrmScarlet.* Right: *gfp::tev::flag::prg-1;lmn-1::wrmScarlet.*

(C) Gene ontology enrichment analysis of the P granule proteome performed using Metascape.

(D) Pie chart summarizing the conservation statistics of P granule proteins.

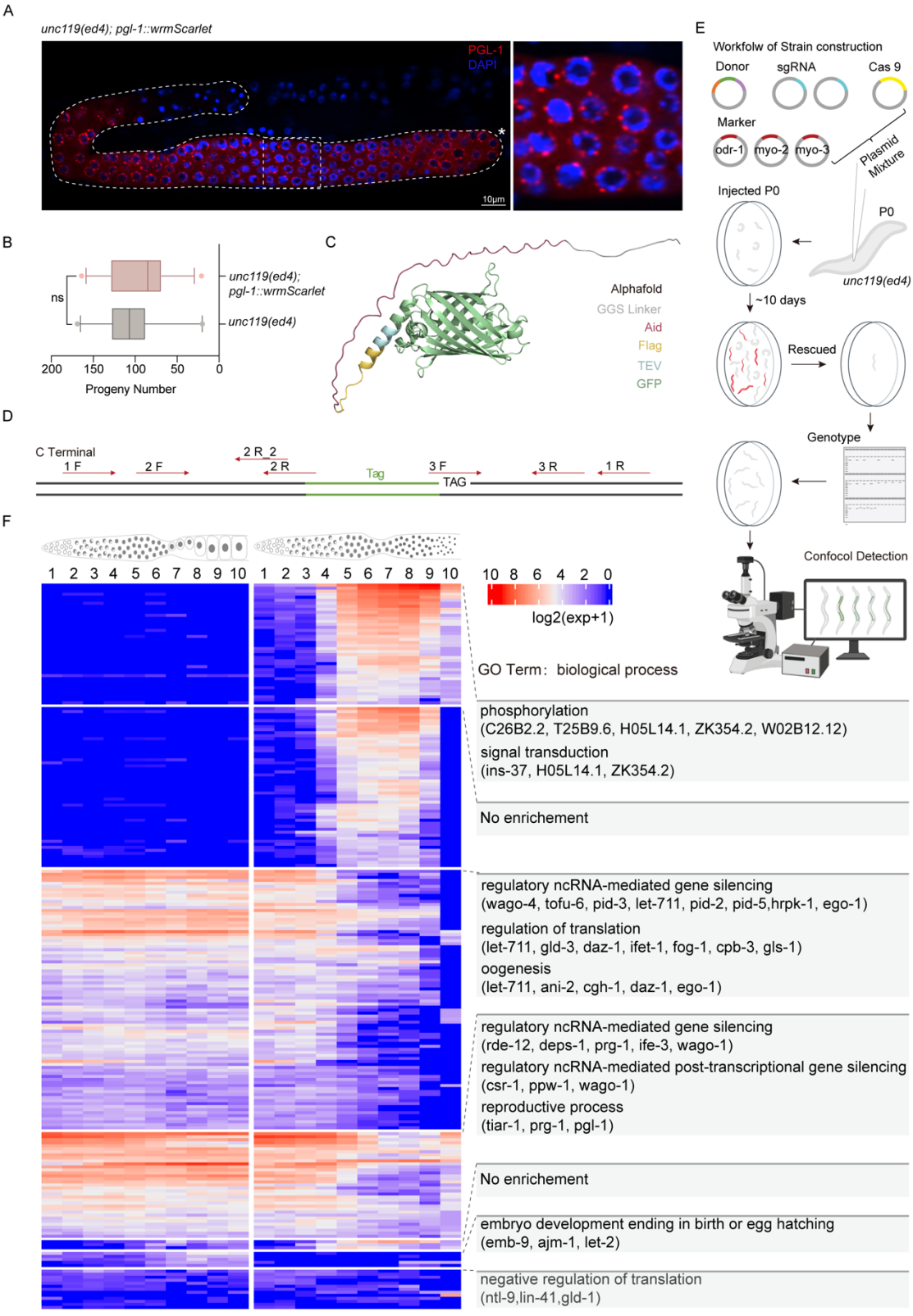

Supplementary Figure 2: Endogenous tagging of P granule proteins and their transcriptional expression trajectories

(A) Representative confocal images of wrmScarlet labeled PGL-1in *unc119 (ed4)* strains.

(B) Quantification of progeny numbers for *unc-119(ed4)* and *unc-119(ed4); pgl-1::wrmScarlet*

strains. n.s., no significant difference.

(C) Structural model of the multifunctional tag predicted by AlphaFold.

(D) Schematic workflow of the large-scale endogenous tagging process.

(E) Schematic showing primers required for construction of the C-terminal donor plasmid.

(F) Each row represents a single P granule gene, and expression levels are displayed as normalized z-scores. Sections 1–10: from the distal mitotic tip (section 1), through the different developmental stages, to the final mature gametes (section 10).

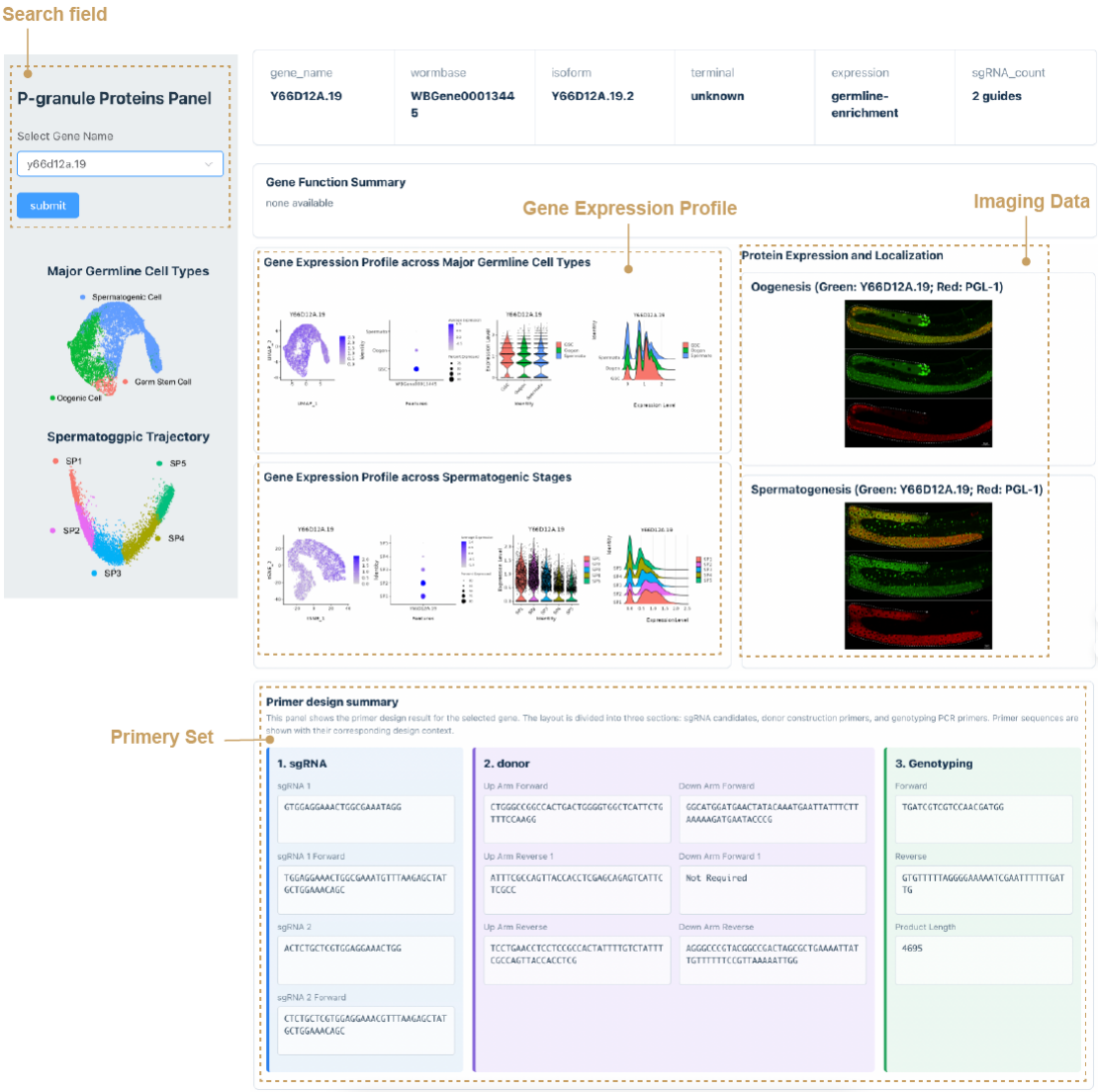

Supplementary Figure 3: Screenshot of the searchable online database for P-granule proteins

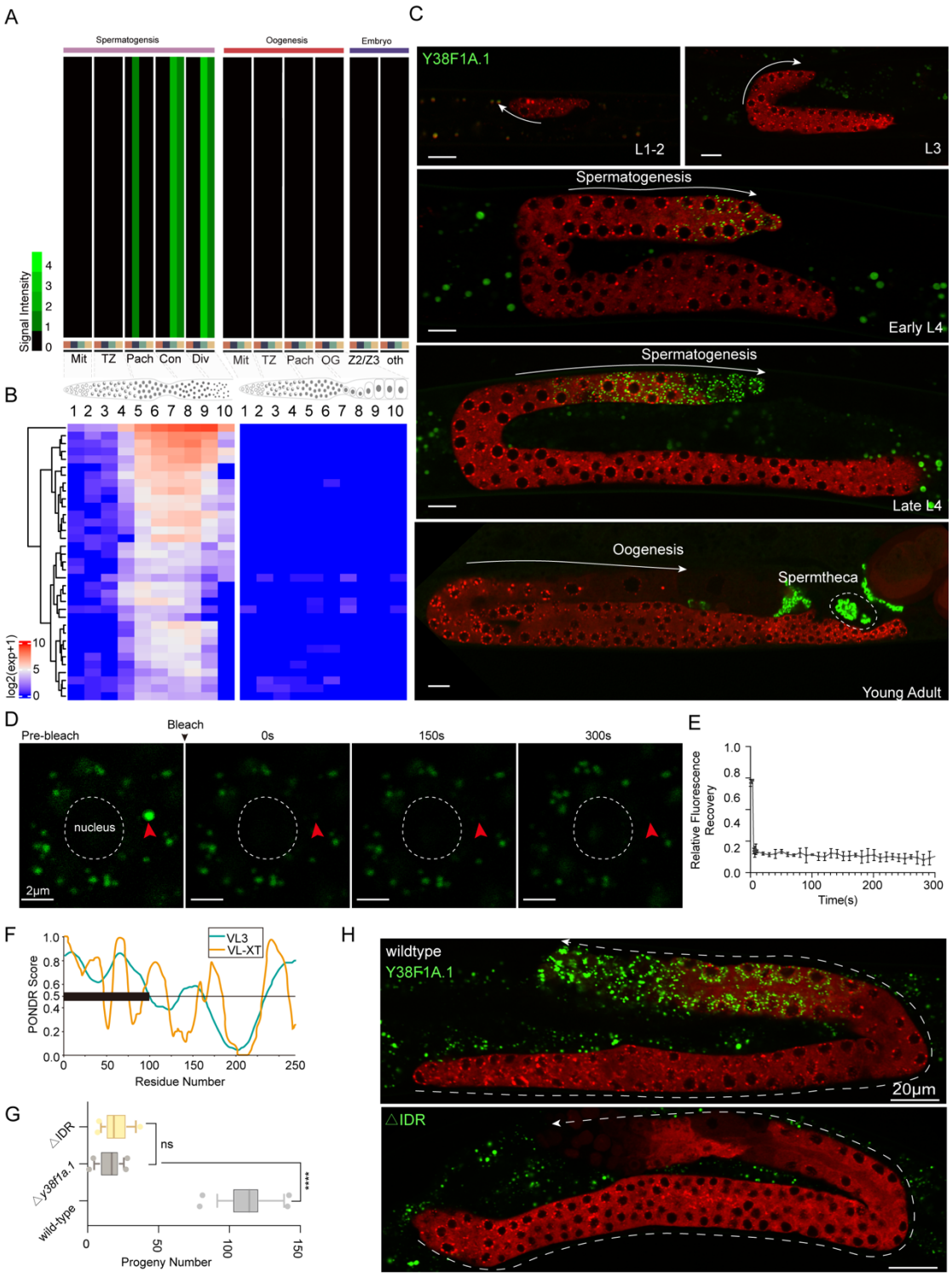

Supplementary Fig 4: Features of functional sperm specific granules

(A) Heatmap showing localization trajectories of sperm granule proteins during development. Red squares: nuclear diffuse signal; blue squares: perinuclear granule signal; green squares: cytoplasmic granule signal; yellow squares: cytoplasmic diffuse signal. Mit: mitotic region; Tran: transition zone; Pach: pachytene region; Con: condensation zone; Div: division zone; OG: oogenesis; Oth: other region. Color scale: 0, no signal; 1, weak; 2, detectable; 3, significant; 4, strong.

(B) Heatmap showing transcriptional expression trajectories of sperm granule proteins during gametogenesis. Sections 1–10: from the distal mitotic tip (section 1), through the different developmental stages, to the final mature gametes (section 10).

(C) Representative confocal images showing the expression pattern of Y38F1A.1 across development. *pgl-1::wrmScarlet* serves as a P granule marker. Scale bars: 10 μm.

(D) Time-lapse confocal images showing fluorescence recovery of Y38F1A.1 after photobleaching.

(E) Quantification of FRAP results. Data were obtained from five cells per group and are presented as mean ± SEM (error bars).

(F) Y38F1A.1 domain composition. Prediction of intrinsically disordered regions was performed using PONDR VSL2 and PONDR VL3 algorithms.

(G) Brood size of wild-type and Y38F1A.1 variants. ****p<0.0001, two-tailed Student's t-test.

(H) Confocal images of late-L4 stage hermaphrodites expressing indicated proteins. In all images: Green: Y38F1A.1, Red: PGL-1. Images represent two biologically independent experiments.

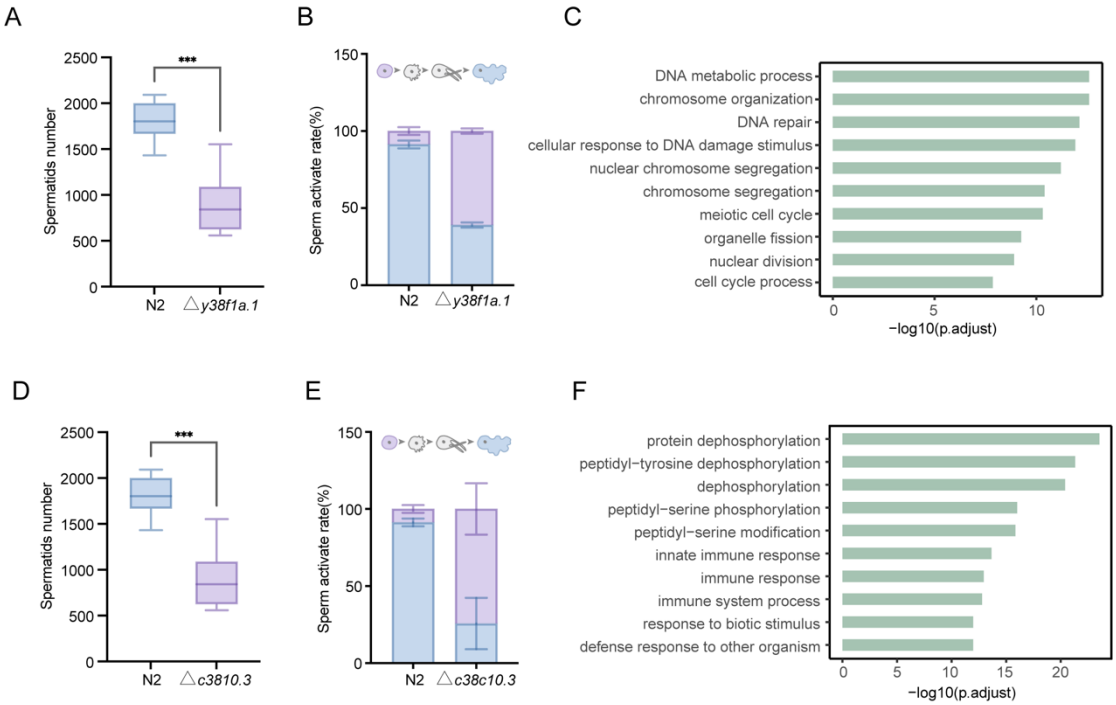

Supplementary Fig 5: Sperm-specific germ granules participate in diverse functions that synergistically promote spermatogenesis.

(A, D). Quantification of sperm numbers in *Y38F1A.1* (A) and *C38C10.3* (D) knockout mutants. $^{**}p \leq 0.001$; $^{***}p \leq 0.0001$.

(B, E). In vitro sperm activation assays for *Y38F1A.1* (B) and *C38C10.3* (E) knockout mutants.

(C, F). Gene Ontology (GO) analysis of downregulated genes identified by RNA-seq from *Y38F1A.1* (C) and *C38C10.3* (F) knockout mutants. RNA samples were obtained from round spermatids (C) and late L4-stage gonads (F). Adjusted $p < 0.05$.